Robust, Accurate, and Fast Decentralized Power Sharing Mechanism for Isolated DC Microgrid Using Droop-Based Sliding-Mode Control

Mohammad Veysi, Jamshid Aghaei, *Senior Member, IEEE*, Mohammad Reza Soltanpour, Mokhtar Shasadeghi, Behrooz Bahrani, *Senior Member, IEEE*, and Daniel Joseph Ryan, *Student Member, IEEE*

***Abstract*—In this paper, a droop-based sliding mode controller (DBSMC) is designed for power sharing in an isolated DC microgrid (DC MG), with improved nonlinear droop model, in the presence of bounded structured uncertainties and external disturbances. The proposed DBSMC strategy does not require any communication link. The design process of the proposed controller is such that the trade-off between the two factors proportional power sharing and precise voltage regulation reaches the minimum possible. The creative design of the controller greatly reduced the control action stress, in such a way that, the occurrence of various uncertainties in the nonlinear droop model is compensated by applying small intelligent changes in the control parameters, using a fuzzy approximator. To evaluate the efficiency of the designed DBSMC controller, simulations are performed on an isolated DC MG with DC-DC buck configuration in MATLAB software. Finally, the real-time digital simulation results utilizing real-time digital power system simulator (RTDS) corroborate the performance of the proposed DBSMC controller. The simulation results obtained from MATLAB and the RTDS verify the robust, accurate and fast function of the proposed droop-based controller in power sharing of the isolated DC MG in the presence of variable operating conditions, parametric uncertainties and external disturbances.**

***Index Terms*—Droop-based sliding mode control (DBSMC), fuzzy approximator, power sharing, improved nonlinear droop model, DC-DC buck converter, isolated DC MG.**

NOMENCLATURE

K_d	Droop coefficient
V_{op}	Operating point voltage (V)
I_{op}	Operating point current (A)
ΔV_o	The variations of the output DC voltage (V)
ΔP	The variations of the instantaneous power (W)
V_o^*	Reference voltage (V)
I^*	Reference current (A)
V_i^*	Control input (V)
V_{E_n}	Nominal DC source voltage (V)
ΔV_E	The variations of the DC source voltage (V)
R	Load (Ω)
R_L	Line resistance (Ω)
R_{dg}	The internal resistance of the converter (Ω)
ΔI_{dg}	The variations of the converter internal resistance current (A)
ΔI_L	The variations of the converter inductance current (A)
ω_c	Angular frequency (cutoff frequency) (rad/s)
K_{Pv}	The proportional gain of the voltage controller
K_{Iv}	The integral gain of the voltage controller
K_{Pi}	The proportional gain of the current controller
K_{Ii}	The integral gain of the current controller.

I. INTRODUCTION

SINCE the late of the 20th century, the continuous expansion of power semiconductor devices and power converters, provides the feasibility of supple current/voltage transformation and hence reinstates DC power to the original position finding its uses [1]–[3]. It can be said that the "War of the currents" is not over yet and T. Edison's victory over G. Westinghouse and N. Tesla is finally happening during the time! DC MGs are distinguished by attractive features such as high system efficiency and reliability, high power quality, economic and largely autonomous operation, low conversion stages, and less complex control and management [4]. Many control strategies and power management methods have been suggested to obtain desirable DC MG operation, in various challenging operating conditions and in the presence of structured uncertainties and external disturbances [5]. At the moment of the occurrence the adverse operation situations and uncertainties, the proportional load sharing is a crucial issue to avoid unfavorable overloading and achieving precise voltage regulation [5], [6].

Manuscript received 25 April 2021; revised 10 September 2021, 5 December 2021, 13 January 2022, and 17 February 2022; accepted 5 March 2022. Date of publication 7 July 2022; date of current version 21 October 2022. Paper no. TSG-00650-2021. *(Corresponding author: Jamshid Aghaei.)*

Mohammad Veysi and Mokhtar Shasadeghi are with the Department of Electrical and Electronics Engineering, Shiraz University of Technology, Shiraz 71557-13876, Iran (e-mail: m.veysi@sutech.ac.ir; shasadeghi@sutech.ac.ir).

Jamshid Aghaei is with the Department of Electrical and Electronics Engineering, Shiraz University of Technology, Shiraz 71557-13876, Iran, and also with the Department of Electrical Engineering, School of Energy Systems, Lappeenranta University of Technology, 53850 Lappeenranta, Finland (e-mail: jamshid.aghaei@lut.fi).

Mohammad Reza Soltanpour is with the Department of Electrical Engineering, Aeronautical University of Science and Technology, Tehran 1384673411, Iran (e-mail: soltanpour@ssau.ac.ir).

Behrooz Bahrani and Daniel Joseph Ryan are with the Department of Electrical and Computer Systems Engineering, Monash University, Melbourne, VIC 3800, Australia (e-mail: behrooz.bahrani@monash.edu; daniel.joseph.ryan@monash.edu).

Color versions of one or more figures in this article are available at https://doi.org/10.1109/TSG.2022.3181494.

Digital Object Identifier 10.1109/TSG.2022.3181494

One of the simplest and most widely developed techniques of decentralized control for AC and DC MGs is droop control [6], [7]. In isolated mode of DC MGs operation, linear P-V droop control shares DGs power proportionally based on DGs power ratings and regulates the DC terminal voltage accurately, using local measured MG state variables as the control parameters [5]–[10]. Despite these advantages, there is low accuracy of power sharing, due to line parameters and sensor errors. The quantitative impact of line resistance on the load sharing and voltage regulation in DC MGs has been expressed in [6], [11]. Therefore, the essential need to improve conventional droop technique is undeniable. Initial efforts in this area include: increasing the droop resistance [11], inserting the additional virtual output impedance [12], injection a small AC signal for active power sharing coordination, using frequency [13], and etc. Unfortunately, these methods did not succeed in solving the problem, for obvious reasons. The conventional droop method can be improved using adaptive determination of the droop coefficients, based on the changes of the DC MG parameters [14]. Another control tendencies are defining the rules in the form of linear controllers to change the droop resistances in accordance with the system changes, to satisfy the system's objectives [15], [16]. These linear rule-based approaches do not present the accurate droop coefficient compensation, due to the lack of intelligence and automaticity. A low bandwidth communication network can improve the load sharing accuracy [17]. In [18], a two-level control technique is suggested for an islanded DC MGs, in such a way that, a P-V droop strategy and a voltage derivative restoration mechanism are utilized as primary and secondary control; respectively. However, the existence of communication network in the DC MG structure can increase the cost and stabilization time as well as reduce the reliability. In [19], a virtual voltage-based droop control technique is designed to reduce the voltage deviation and achieve proportional power sharing. In [20], an attractive frequency-based droop strategy is presented for power sharing in DC microgrids with various low, medium and high X/R ratios. These researches haven't enough robustness against the generation side uncertainties such as DG outage and DG voltage variations. In [21], a hierarchical control structure with a novel dynamic droop coefficient correction control is introduced to achieve precise power sharing in DC microgrids. Unfortunately, in this control structure, high dependence on communication links degrades the reliability and efficiency of the system. In [22], more than ten recently proposed decentralized droop control strategies are comprehensively reviewed, and their innovations are expressed. A closer study of these strategies can pave the way for valuable future researches. In [5], a droop-based T-S fuzzy sliding mode controller is designed to proportional power sharing of isolated boost converter-based DC MG, using the equivalent T-S fuzzy model. The DGs voltage variations are not considered. The long transient-states of the DGs output powers and DC bus voltage, oscillatory DC voltage convergence in the uncertainties occurrence moments as well as the slow and gradual convergence of the DGs output powers to the proportional power values, are the other weaknesses.

In this paper, to reduce related problems with linear P-V droop control, an improved nonlinear droop model for isolated buck converter-based DC MG is obtained using the expressed concepts in [5], [6]. Next, a DBSMC controller is designed, in such a way that, two state variables DG output power and DC terminal voltage are controlled with only one control input, in the presence of variable operating conditions, bounded structured uncertainties and external disturbances. The DBSMC control parameters are approximated using a low computational load fuzzy approximator. The basis of the fuzzy approximator function is defining the proper criteria in order to tracking error evaluation.

According to the above descriptions, this paper presents a novel nonlinear robust, accurate and fast DBSMC controller, to achieve proportional power sharing. The performance and creative design procedure of the proposed nonlinear robust droop control strategy represents the extraordinary role of three following significant factors in the proportionality, accuracy and rapidity in power sharing of isolated DC MGs, in the presence of the various uncertainties: a) considering the nonlinear terms in droop modeling, b) minimization the trade-off between the proportional power sharing and precise voltage regulation, and c) reducing the computational load of the control input. In fact, mentioned features bring the ability to implement the proposed control in practice.

The rest of the paper is organized as follows: Section II expresses the modeling procedure of the improved droop strategy. In Section III, a DBSMC controller is designed and the global asymptotic stability of the closed-loop system will be proved. Next, a low computational load fuzzy approximator is introduced for approximation of the control parameters. Section IV clarifies the steps to design and advantages of the proposed DBSMC controller in detail. In Section V, to demonstrate and to compare the function of the proposed DBSMC controller, simulations are conducted on an isolated buck converter-based DC MG in MATLAB software. Furthermore, real-time simulation results attained from an RTDS system are given. Eventually, conclusions are presented in Section VI.

II. Modeling of Improved Droop Strategy

In fact, the improved droop strategy is utilized to control the DC-DC converters, which act as interface equipment for DGs and DC MG. The improved droop method can be used for converters with different topologies. For example, in [5] all converters have boost structure. In this paper, all converters are considered with a buck configuration. Using the advantages of the droop strategy model and DC-DC converter components such as voltage and current controllers, small-signal analysis can be utilized. According to the concepts presented in [5], [23], and [24], the general block diagram of the system is shown in Figure 1. The function of this block diagram can be expressed according to the following steps:

1. The output voltage and current of the converter (V_o, I_o) are applied as input to the power control block. In this block, the calculated power (p_{in}) passes through a low-pass filter and the average power (p) is extracted. Average power is exerted

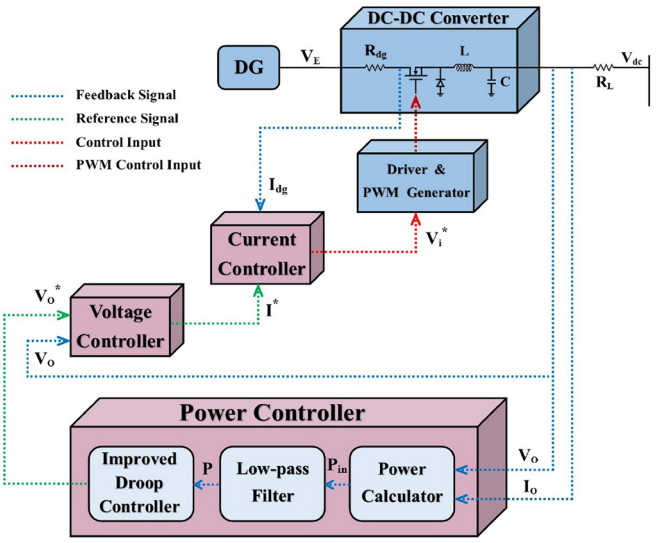

Fig. 1. General schematic representation of VSI.

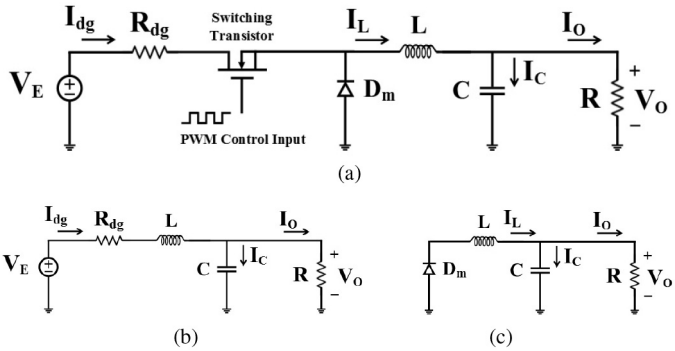

Fig. 2. Circuit structure and operating modes of the DC-DC buck converter (a) buck converter circuit (b) operating mode 1, $V_i^* = 1$, $PWM \rightarrow High$ (c) operating mode 2, $V_i^* = 0$, $PWM \rightarrow Low$.

to the improved droop controller in the power controller to achieve the desired power sharing. The output of the droop controller is the reference voltage (V_o^*).

2. The output voltage of the converter and the output of the power control block (reference voltage) are applied as input to the voltage control block. The output of the voltage controller block is the reference current signal (I^*).

3. The output of the voltage controller block (reference current) and the converter input current (I_{dg}), which is actually the current due to the internal resistance of the converter (R_{dg}), are applied as input to the current controller block. The output of the current controller block is the voltage signal (V_i^*) input to the power switch driver, as the PWM pulse generator.

The linearized model of the system around the operating point (V_{op}, I_{op}), which is the output voltage and current of the converter at the operating point, is utilized to analyze the small-signal stability of the system in Figure 1, according to the following equation [5], [23]:

$$\Delta\dot{P} = -\omega_c \Delta P + \omega_c I_{op} \Delta V_o + \omega_c V_{op} \Delta I_o \tag{1}$$

where ω_c is the angular frequency of the filter.

In the above relation, ΔP and ΔV_o are considered as state variables. Next, the variables Ψ and Γ are marked to describe the voltage and current control loops, respectively [5], [6]:

$$\Delta\dot{\Psi} = \sqrt{\Delta P/K_d + 0.25V_{op}^2} - 0.5V_{op} - \Delta V_o \tag{2}$$

$$\Delta\dot{\Gamma} = K_{Iv}\Delta\Psi - \Delta I_{dg} - K_{Pv}\Delta V_o + K_{Pv}\left(\sqrt{\Delta P/K_d + 0.25V_{op}^2} - 0.5V_{op}\right) \tag{3}$$

where K_d signifies the suggested droop coefficient.

As mentioned before, in this paper, all converters are considered with buck structure. Therefore, in the following, the performance of the buck converter and its two operating modes will be briefly reviewed. The structure of the DC-DC buck converter and its two operating modes are shown in Figure 2. To describe the converter dynamics, analysis of its operating modes is necessary. According to Figure 2-(a), the buck converter has a power transistor and a flywheel diode. The first operating mode, Figure 2-(b), occurs when the PWM pulse stands high. Also, the second operating mode, Figure 2-(c), arises when the PWM pulse is low. As is clear, in the first operating mode, the power transistor is on and the flywheel diode is off, and vice versa, in the second operating mode, the power transistor is off and the flywheel diode is on, to direct the energy stored in the inductor L. The circuits of Figures 2-(b) and 2-(c) have one node. By KCL at these nodes and also using KVL around the outer loops of these circuits we will have the following relations:

$$KVL\begin{cases} Mode\ 1: V_i^* = 1,\ -V_E + R_{dg}I_{dg} + V_L + V_O = 0 \\ Mode\ 2: V_i^* = 0,\ V_L + V_O = 0 \end{cases} \tag{4}$$

$$KCL\begin{cases} Mode\ 1: V_i^* = 1,\ I_C = I_{dg} - I_O;\ \ I_{dg} = I_L \\ Mode\ 2: V_i^* = 0,\ I_C = I_L - I_O;\ \ I_{dg} = 0 \end{cases} \tag{5}$$

Now, considering that the value of the variable V_i^* is zero or one, the above relations can be combined as follows, so that the following relations represent both operating modes of the buck converter:

$$KVL:\ -V_i^*V_E + V_i^*R_{dg}I_{dg} + V_L + V_O = 0 \tag{6}$$

$$KCL:\ I_C = V_i^*I_{dg} + \left(1 - V_i^*\right)I_L - I_O \tag{7}$$

The behavior model of DC-DC buck converter circuit can be extracted from (6) and (7) as follows:

$$dI_L/dt = \left[V_i^*V_E - V_i^*R_{dg}I_{dg} - V_O\right]/L \tag{8}$$

$$dI_{dg}/dt = V_i^*\left[V_i^*V_E - V_i^*R_{dg}I_{dg} - V_O\right]/L \tag{9}$$

$$dV_O/dt = \left[V_i^*I_{dg} + \left(1 - V_i^*\right)I_L - I_O\right]/C \tag{10}$$

Finally, the state-space representation of the overall system equations can be obtained, in the format $\dot{X} = f(x) + g(u)$, using (1-3) and (8-10) as:

$$\begin{bmatrix} \Delta\dot{P} \\ \Delta\dot{\Psi} \\ \Delta\dot{\Gamma} \\ \Delta\dot{I}_L \\ \Delta\dot{I}_{dg} \\ \Delta\dot{V}_o \end{bmatrix} = f(x) + \begin{bmatrix} \omega_c V_{op}\Delta I_o \\ 0 \\ 0 \\ 0 \\ 0 \\ -\frac{1}{C}\Delta I_o \end{bmatrix} \tag{11}$$

The $f(x)$ as a 6×1 vector is addressed in Appendix A.

The nonlinearity of the state-space equations (11) is obvious. In fact, the DG voltage and the load size are uncertain. In addition, the existence of uncertainty in the feedback signals V_o and I_o, as well as I_{dg}, cannot be denied. Therefore, controlling this system with a conventional PI controller is a very challenging issue and designing a robust nonlinear controller seems very essential.

Remark 1: Voltage and current controllers are usually simple PI controllers.

Remark 2: In this paper, variations of the DC source voltage (ΔV_E) and line resistance (R_L) are considered.

III. Power Sharing Using DBSMC Control

According to the dual purposes of proportional power sharing and precise voltage regulation, the following functions are defined based on the state variables ΔP and ΔV_o expressed in (11):

$$f_1(x_1, x_6) = f(x)_{11} \tag{12}$$

$$g_1 = \omega_c V_{op} \tag{13}$$

$$f_2(x_1, x_2, x_3, x_4, x_5, x_6) = f(x)_{61} \tag{14}$$

$$g_2 = -1/C \tag{15}$$

where $f(x)_{11}$ and $f(x)_{61}$ are the elements of the first and sixth rows of the vector $f(x)$.

Now (12) and (13) as well as (14) and (15) are respectively inserted in the relations related to $\Delta\dot{P}$ and $\Delta\dot{V}_o$, which have been expressed in (11), as:

$$\Delta\dot{P} = f_1(x_1, x_2) + g_1 u(t) \tag{16}$$

$$\Delta\dot{V}_O = f_2(x_1, x_2, x_3, x_4, x_5, x_6) + g_2 u(t) \tag{17}$$

Next, f_1 and f_2 are used instead of $f_1(x_1, x_2)$ and $f_2(x_1, x_2, x_3, x_4, x_5, x_6)$, respectively, for the sake of brevity. In order to realize the proposed improved droop strategy, the following state-space equations are used in the proposed model-based control:

$$\begin{cases} \dot{x}_1 = f_1 + g_1 u(t) + d_1(t) \\ \dot{x}_6 = f_2 + g_2 u(t) + d_2(t) \end{cases} \tag{18}$$

where $d_1(t)$ and $d_2(t)$ represent unmodeled dynamics and external disturbances. To design the proposed controller, the following assumptions must be met [25], [26]:

Assumption 1: All state variables are measurable.

Assumption 2: The functions f_1, f_2, g_1 and g_2 have uncertainty.

Assumption 3: The functions g_1 and g_2 are bounded and non-zero.

Assumption 4: External disturbances are unknown, but their upper bounds are clear, i.e., $\|d_i(t)\| \le d_i^{\max}$.

Remark 3: Explaining assumption 2, it should be noted that $f_i = f_{ci} + f_{ui}$ and $g_i = g_{ci} + g_{ui}$. f_{ci} and g_{ci}, as well as f_{ui} and g_{ui}, are the known and unknown parts of the functions f_i and g_i, respectively. Although the functions f_{ui} and g_{ui} are unknown, the upper bound of f_{ui}, i.e., $f_{ui} \le f_{ui}^{\max}$, is clear. Also, the upper and lower bounds of g_{ui}, i.e., $0 < g_{ui}^{\min} \le g_{ui} \le g_{ui}^{\max}$, are specified.

Next, the state-space equations (18) are transferred to the error domain. So, the following definitions are provided:

$$\begin{cases} e_1 = x_1 - x_{d1} \\ e_6 = x_6 - x_{d6} \end{cases} \tag{19}$$

where x_{d1} and x_{d6} are desirable values, that must be followed by the state variables x_1 and x_6, respectively. e_1 and e_6 are also tracking errors. Next, equations (19) are derived with respect to time and then equations (18), considering Remark 3, are placed in them:

$$\begin{cases} \dot{e}_1 = \dot{x}_1 - \dot{x}_{d1} = f_{c1} + g_{c1} u(t) + D_1(t) - \dot{x}_{d1} \\ \dot{e}_6 = \dot{x}_6 - \dot{x}_{d6} = f_{c2} + g_{c2} u(t) + D_2(t) - \dot{x}_{d6} \end{cases} \tag{20}$$

where $D_1(t)$ and $D_2(t)$ are considered as total disturbances and defined as:

$$\begin{cases} D_1(t) = f_{u1} + g_{u1} u(t) + d_1(t) \\ D_2(t) = f_{u2} + g_{u2} u(t) + d_2(t) \end{cases} \tag{21}$$

In fact, equations (20) are state-space equations in the error domain.

Assumption 5: According to Assumption 4 and Remark 3, as well as due to control input $u(t)$ being bounded [27], the upper bounds of introduced total disturbances (21) are clear, i.e., $\|D_i(t)\| \le D_i^{\max}$.

Remark 4: As shown in (20), the system has only one control input $u(t)$. Controlling two state variables x_1 and x_6 of the nonlinear system with one control input seems challenging.

A. DBSMC Controller Design

In order to control the system (20), a DBSMC controller is proposed. For this purpose, the following sliding surfaces are defined [27]:

$$\begin{cases} s_1 = \xi e_1 \\ s_2 = \zeta e_6 \end{cases} \tag{22}$$

where ξ and ζ are positive constants. Equivalent control inputs are selected as follows:

$$\begin{cases} u_{eq1}(t) = -\frac{1}{g_{c1}}(f_{c1} + \xi e_1) \\ u_{eq2}(t) = -\frac{1}{g_{c2}}(f_{c2} + \zeta e_6). \end{cases} \tag{23}$$

Theorem 1: In the state-space equations (20), if control input $u(t)$ is selected as follows, the tracking errors e_1 and e_6 asymptotically converge to zero with any initial condition:

$$u(t) = u_{eq1}(t) + u_{eq2}(t) + u_s(t)$$

$$u_s(t) = \frac{-1}{\begin{Bmatrix} \xi g_{c1} \\ +\zeta g_{c2} \end{Bmatrix}} \begin{Bmatrix} \left(\xi g_{c1} + \zeta g_{c2}\right)\begin{pmatrix} u_{eq1}(t) \\ +u_{eq2}(t) \end{pmatrix} \\ +\xi f_{c1} + \zeta f_{c2} - (\xi \dot{x}_{d1} + \zeta \dot{x}_{d6}) \\ +kS + \rho sat(S) \end{Bmatrix} \tag{24}$$

where k and ρ are positive constants.

The proof of Theorem 1 is given in Appendix B.

B. Fuzzy Approximation of SMC Coefficients

Usually, SMC coefficients are determined and adjusted by trial and error. Here, a fuzzy approximator system is used to determine the control coefficients ξ and ζ. At first, the initial parameters ξ_0 and ζ_0, determined by the designer based on

known system information, are applied to the DBSMC controller. Then, according to the evaluation of the controller performance and the effects of the previous approximation (initializing in the first step), the controller parameters are approximated again. In fact, the performance of the sliding mode controller can be evaluated from two aspects of control input chattering phenomenon and tracking error. Due to the use of the $sat(S)$ function in the design process of the sliding mode controller, the problem of control input chattering has been solved. Next, the tracking error evaluation criterion ($TEEC$) is used to evaluate the controller performance in relation to the tracking error:

$$TEEC = \frac{\lambda \int_0^T |e| dt}{\int_0^T |x_d| dt} \tag{25}$$

where $e = x - x_d$ represents the tracking error, T is the approximation time interval, and λ is a positive constant. Indeed, this description indicates that the tracking error must be evaluated according to the reference input amplitude. As a result, better tracking can be expected from the controller by tending $TEEC$ to zero.

Here, the problem of approximation of sliding mode control parameters is considered as a solution search procedure in the form of a fuzzy intelligent optimization problem in order to minimize the $TEEC$ criterion. In the following, for easier expression of the content, parameters ξ and ζ are briefly introduced with parameter p. In the intended optimization problem, for each initial value of the p parameter (p_0), the desired value of the p parameter (p_d), which minimizes the $TEEC$ criterion, is obtained. The fuzzy intelligent minimization process, until the value of p_d is attained for the minimum value of the $TEEC$ criterion ($TEEC_{\min}$), is repeatedly searched for the p parameter using the following relation:

$$p_{i+1} = p_i + \Delta p_i \tag{26}$$

At each approximation step, Δp is achieved according to the effect of the previous approximation. Due to the fact that the parameters of the proposed DBSMC controller (ξ, ζ) are positive constants, if p_0 is greater than p_d, Δp is a negative number, and if p_0 is less than p_d, Δp will be a positive number. $\Delta TEEC$ is also defined according to the value of $TEEC_{\min}$ as determined by the controller designer. Therefore, the following relations represent $\Delta TEEC$ and Δp:

$$\begin{cases} \Delta p = p_d - p_0 \\ \Delta TEEC = TEEC_{\min} - TEEC_0 \end{cases} \tag{27}$$

$\Delta TEEC$ is always a negative or zero value. Figure 3(a) provides a visual representation of the minimum value search process in the proposed intelligent minimization method. Different values and signs of Δp, as well as different values of $\Delta TEEC$, create distinctive search paths in the diagram of Figure 3(a), which can be represented as Figure 3(b).

Here, Δp and $\Delta TEEC$ represent the changes in the value of the p-parameter and changes in the $TEEC$ criterion during the approximation process, respectively. Next, $\Delta TEEC/\Delta p$ is defined as the sensitivity factor for approximating the p parameter, where, $\Delta TEEC = TEEC_{new} - TEEC_{old}$ and

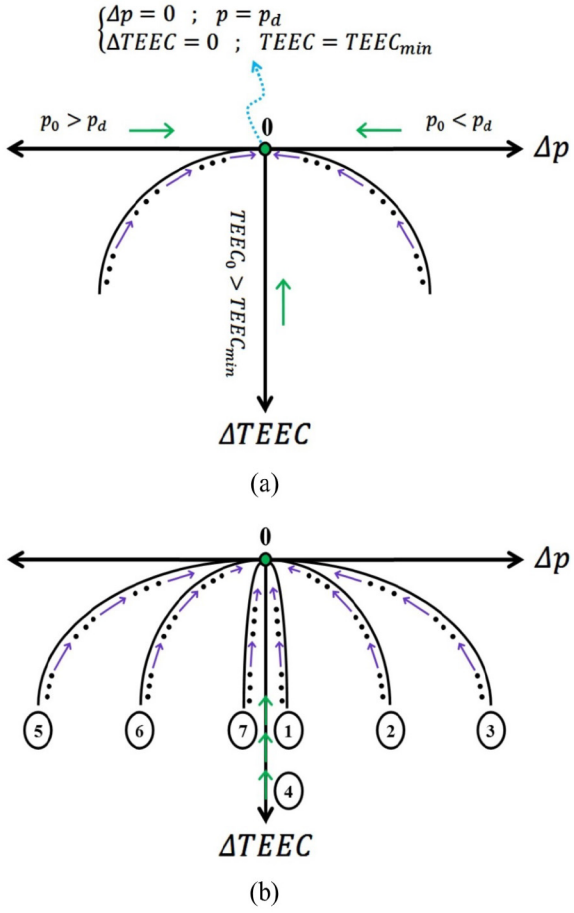

Fig. 3. Visual representation of the proposed intelligent minimization method (a) minimum value search process (b) distinctive search paths.

$\Delta p = p_{new} - p_{old}$. The sensitivity factor indicates how sensitive the control performance is to the control parameter approximation. If the value of this factor is considered large, in the next step of approximation, there will be a small change in the value of the control parameter and vice versa. Carefully in Figure 3-(b), this concept is easily understood.

To guarantee the stability and increase the accuracy of the proposed DBSMC controller, the parameters ξ and ζ must be approximated. This approximation can be defined as the process of searching for the values of the control parameters to minimize the $TEEC$ criterion. The flowchart of the execution process of the proposed algorithm is shown in Figure 4.

Remark 5: The proposed algorithm is separately implemented to approximate both control parameters ξ and ζ. That is, for the parameter ξ the $TEEC_\xi$ criterion is defined according to the state variable x_1 and for the parameter ζ, the $TEEC_\zeta$ criterion is defined based on the state variable x_6.

Remark 6: In the flowchart of Figure 4, the DGRP is the reference signal for the power of i^{th} DG. In fact, the occurrence of one of the two conditions; a) changing the level of the reference signal for the power of i^{th} DG and, b) the largeness of the $TEEC$ criterion relative to $TEEC_{\min}$, or the simultaneous occurrence of both conditions, are the conditions for parameter re-approximation.

To describe the seven hypothetical paths of the search process in Figure (3-b), the following fuzzy rules can be defined,

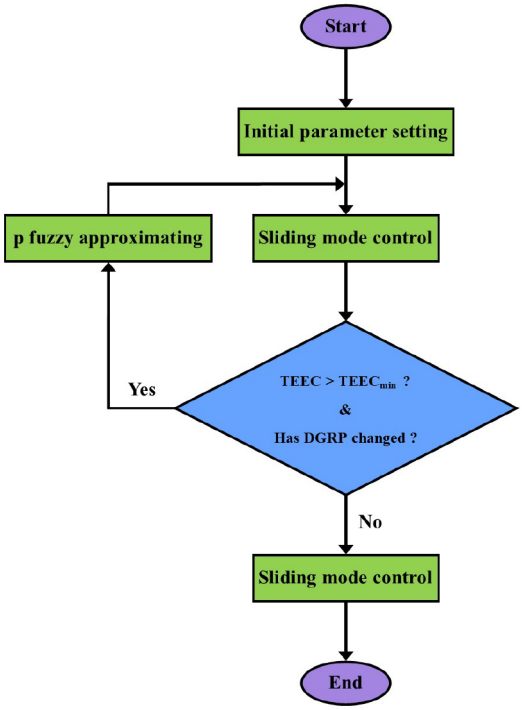

Fig. 4. Flowchart of the proposed algorithm for approximating the control parameters ξ and ζ.

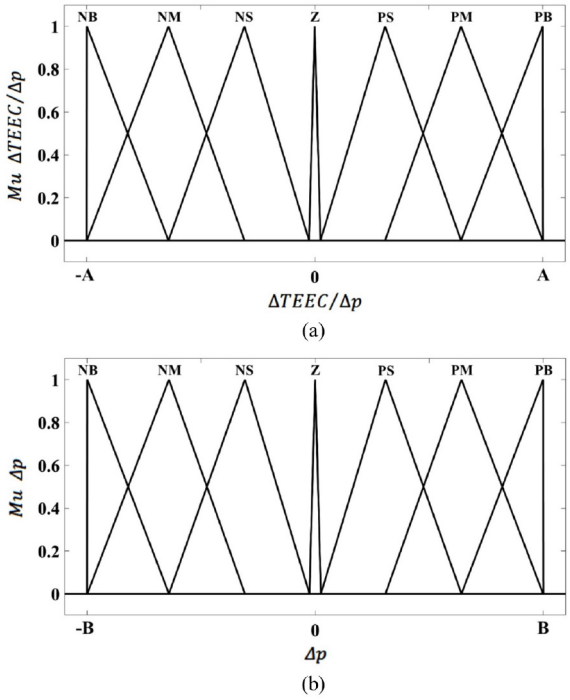

Fig. 5. Fuzzy membership functions (a) membership functions for input variable $\Delta TEEC/\Delta p$ (b) membership functions for output variable Δp.

for each path, respectively:

$$\begin{cases} if\ \Delta TEEC/\Delta p\ is\ NB,\ then\ \Delta p\ is\ PS \\ if\ \Delta TEEC/\Delta p\ is\ NM,\ then\ \Delta p\ is\ PM \\ if\ \Delta TEEC/\Delta p\ is\ NS,\ then\ \Delta p\ is\ PB \\ if\ \Delta TEEC/\Delta p\ is\ Z,\ then\ \Delta p\ is\ Z \\ if\ \Delta TEEC/\Delta p\ is\ PS,\ then\ \Delta p\ is\ NB \\ if\ \Delta TEEC/\Delta p\ is\ PM,\ then\ \Delta p\ is\ NM \\ if\ \Delta TEEC/\Delta p\ is\ PB,\ then\ \Delta p\ is\ NS \end{cases} \quad (28)$$

It should be noted that, in each of the above fuzzy rules, $\Delta TEEC/\Delta p$ is considered as an input variable and Δp as an output variable. Using these fuzzy rules, the controller considers the effect of the approximation of the parameter p and decides on the value of the next approximation. Finally, the value of the parameter p that minimizes the *TEEC* criterion is searched. The membership functions used in the Mamdani fuzzy inference system are shown in Figure 5.

IV. Steps to Design and Advantages of the Proposed DBSMC Controller

A. Steps to Design of the Proposed DBSMC Controller

Briefly, the design process of the proposed DBSMC controller includes the following steps:

1. Define the functions f_1, g_1, f_2 and g_2 according to the (11).
2. Determine the state-space equations (18).
3. Determine the state-space equations in the error domain consistent with (20).
4. Define the sliding surfaces s_1 and s_2 based on (22).
5. Determine the equivalent control inputs $u_{eq1}(t)$ and $u_{eq2}(t)$ according to the (23).
6. Determine the switching control input $u_s(t)$ and control input $u(t)$ according to the (24).
7. Determine the positive constants ρ, k and ε.
8. Determine the values $d_1^{\max}$ and $d_2^{\max}$.
9. Initialize the control parameters ξ and ζ and also determine the values $TEEC_\xi$min and $TEEC_\zeta$min.
10. Determine $TEEC_\xi$ and $TEEC_\zeta$ criteria and define the sensitivity factors $\Delta TEEC_\xi/\Delta\xi$ and $\Delta TEEC_\zeta/\Delta\zeta$ according to the (25) and (27), respectively.
11. Describe the fuzzy rules (28) and membership functions.
12. Approximate the control parameters ξ and ζ according to the flowchart of Figure 4.

In order to better understand the proposed control structure, the block diagram of Figure 6 is presented.

B. Advantages of the Proposed DBSMC Controller

In the design of the proposed DBSMC controller, there are some creativities and innovations that are mentioned as follows:

1. The design process of the proposed controller is such that with only one control input, two state variables Δp and ΔV_o are controlled simultaneously and well. In other words, the trade-off between the two factors proportional power sharing and precise voltage regulation reaches the minimum possible. The proposed controller also overcomes all structured uncertainties and external disturbances. In fact, this advantage indicates the robustness and accuracy of the proposed control.
2. a) In the VSI structure, in the PI voltage and current controllers for each DG, the parameters K_{Pv}, K_{Iv}, K_{Pi} and K_{Ii} are determined separately according to the performance of the i^{th} DG and its related converter.

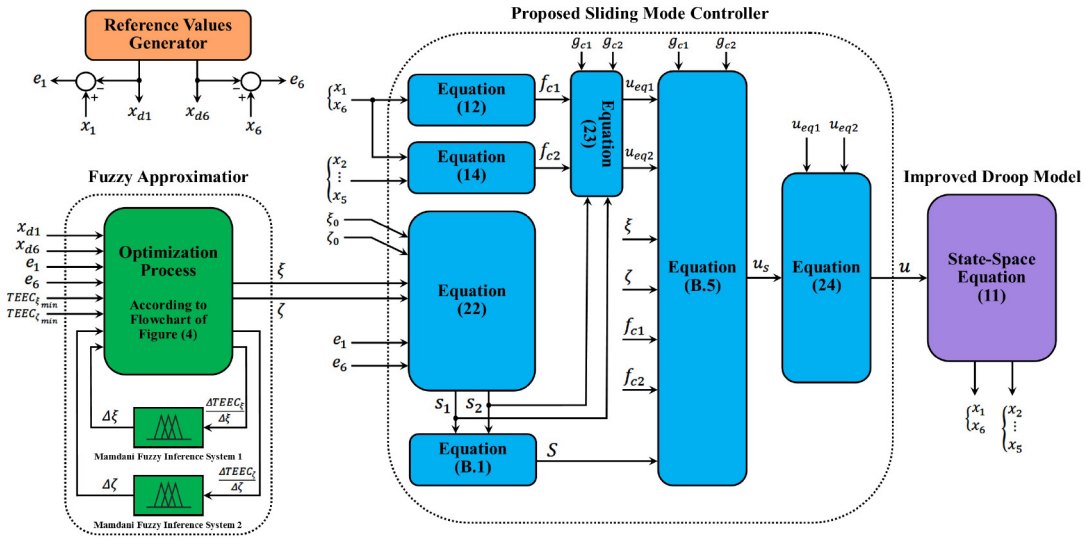

Fig. 6. Block diagram of the proposed control system.

b) According to (11), the presence of $\Delta P/K_d$ is visible in most elements of the vector $f(x)$. Since, by changing the reference power value of DG_i ($P_{i_{ref}}$) or other structured uncertainties occurrence, the value of $\Delta P_i/k_{d_i}$ changes, so we can use the simple relation $k_{d_{inew}} = P_{i_{ref}} * k_{d_{i_{initial}}}/\Delta P_{i_{nominal}}$ to regulate the value of K_d and kept the value of $\Delta P_i/k_{d_i}$ constant.

Due to the above dual features, the control action stress of the proposed DBSMC controller is greatly reduced.

3. Due to the above-mentioned advantage, the occurrence of various uncertainties in the improved droop model is compensated by applying small changes in the control parameters ξ and ζ. Therefore, in the fuzzy approximator, the upper and lower bounds of the membership functions of the input and output variables become smaller, and as a result, the control parameters are approximated very quickly in proportion to the model changes. In fact, this advantage indicates fast and accurate control. In addition, in fuzzy approximator design, single-input, single-output fuzzy rules are used. Also, the fuzzy approximatior rule base has only seven rules. Therefore, due to these features and also due to advantages 1 and 2, the computational load of control input is very small.

4. In the proposed control, the undesirable phenomenon of control input chattering is eliminated, without undermining the proof of the closed-loop system stability.

5. The design process of the proposed DBSMC controller is very simple and also, the performance of the utilized fuzzy approximator is very fast. Therefore, the simplicity, step-by-step nature of the controller design process, as well as the low computational load of the control input, bring the ability to implement the proposed control in practice.

V. Performance Evaluation

A. Simulation Results

In order to evaluate the performance of the proposed DBSMC control, suggested FSMC droop control in [5], the conventional droop method, the droop scheme with virtual resistance and the proposed droop strategy are compared in two cases. As shown in Figure 7, a DC MG consists of three DGs and their respective converters is considered and simulated in MATLAB/Simulink.

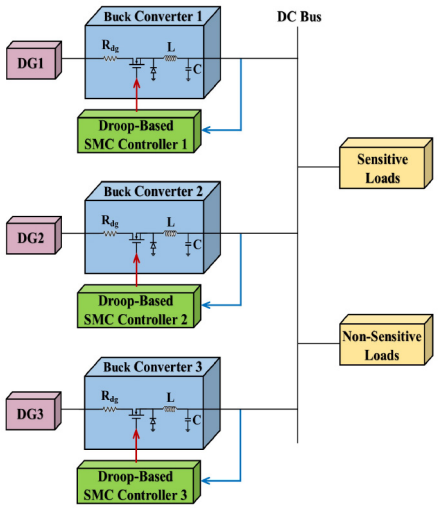

Fig. 7. The configuration of the studied MG.

In two aforementioned cases, the DG nominal ratings are determined as 5kW, 10kW and 15kW for DG1, DG2 and DG3; respectively. Each DG is implemented as a DC power supply, connected to the 400V DC bus using a DC-DC buck converter. For all three DGs V_{E_n}, ΔV_E and V_{op} are 600V, 10V and 400V; respectively. Improved droop model parameters are given in Appendix C. Let us now test the designed DBSMC controller in two cases with various load changes, DG outages, DC source voltage variations and line resistances as follows.

Case 1 (Load Changes, DG Outages and DG Voltage Variations): In this step of the simulation, assumed the load changes from 10kW to 7kW at 0.2s, DG1 removed at 0.6s and DGs voltage variations ΔV_E changed from 10V to 15V at 0.8s. The line resistance values R_{L_1}, R_{L_2} and R_{L_3} are specified

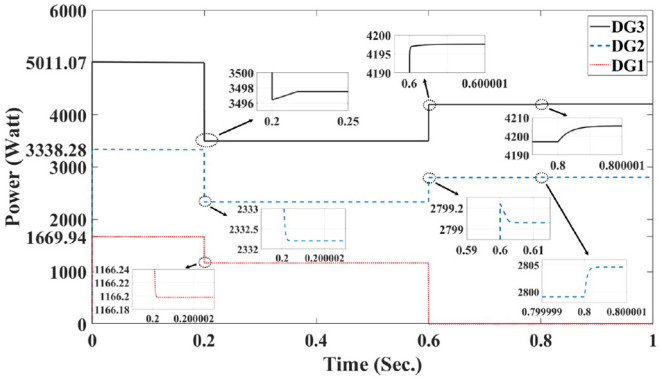

Fig. 8. The power sharing with the proposed DBSMC control in Case 1.

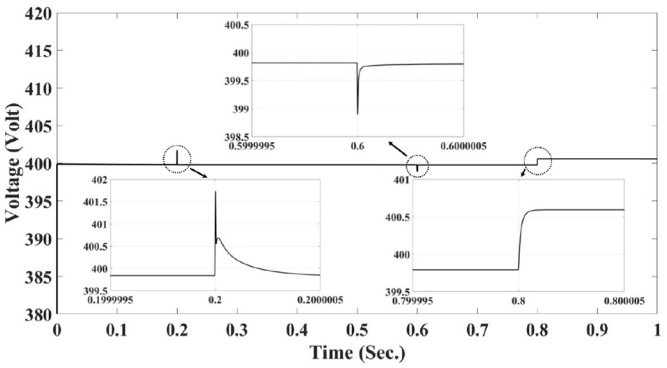

Fig. 9. The DC voltage with the proposed DBSMC control in Case 1.

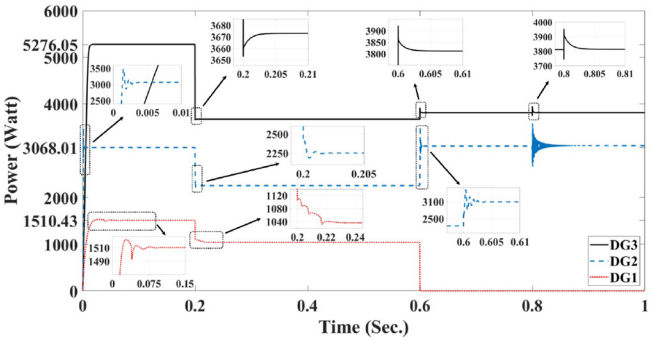

Fig. 10. The power sharing with the droop-based control [5] in Case 1.

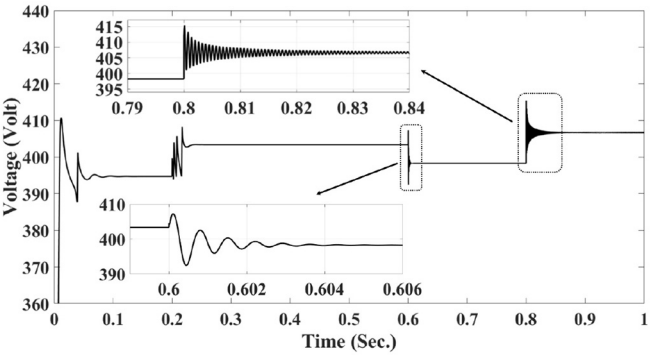

Fig. 11. The DC voltage with the droop-based control [5] in Case 1.

as 0.3Ω, 0.4Ω and 0.5Ω; respectively. According to DGs ratings, the DG1, DG2 and DG3 portions should always be 1:2:3, in the supply of load, under the different conditions of power system working and in the presence of the structured uncertainties and external disturbances. The parameters of the triple DBSMC controllers and the bounds of the fuzzy approximator MFs, indicated in Figure 5, are addressed in Appendix D. Also, the evolution of the fuzzy approximated DBSMC control parameters ξ and ζ are shown in Appendix E. Figures 8 and 9, demonstrated the output powers of the three DGs and the magnitude of the voltage under the proposed DBSMC control. Very short transient-state and the quick readiness of the DGs and their respective converters to provide the load power as well as the rapid convergence of the DGs output powers to the proportional power values, without significant undershoot and/or overshoot, can be seen in Figure 8. The DGs could accurately share the loads, very close to the favorable ratio of 1:2:3, utilized the proposed DBSMC control. This desired performance is achieved in uncertain conditions such as 3kW load reduction at 0.2s, outage of DG1 at 0.6s and 5V increase in range of the input voltage of all converters at 0.8s. Furthermore, for parametric uncertainties, it is assumed that the DC-DC buck converters parameters were 90% of the expressed values in Appendix C, and external disturbances are applied using $d_i(t) = d_i^{\max} sin(10t)$. These parametric uncertainties and external disturbances challenge the voltage and current sensors measured values. In addition, no information exchange takes place between the buck converters, in fact, the proposed droop strategy is a decentralized control without the need for any communication links. The almost precise voltage regulation under the above-mentioned uncertain conditions can be deduced in Figure 9.

In the following, in order to further performance evaluation of the proposed DBSMC controller, T-S fuzzy sliding mode controller (FSMC) designed to control the boost converter-based isolated DC MG in [5] is simulated and applied to the studied buck converter-based isolated DC MG. Figures 10 and 11, shown the output powers of the three DGs and the magnitude of the voltage under the droop-based FSMC control [5]. Carefully in Figure 10 and compare it with Figure 8, the very favorable performance of the proposed DBSMC control can be inferred in comparison with the droop-based FSMC control [5]. So that in Figure 10, long transient-state, slow, oscillatory and non-smooth convergence with considerable undershoot and/or overshoot can be seen in the uncertainties occurrence moments at 0.2s, 0.6s and 0.8s. Also, in Figure 11 the poor voltage regulation is clear compared to the proposed droop control. The output powers of the three DGs under conventional droop control are shown in Figure 12. And the results with the virtual resistance compensation can be seen in Figure 13. The considered droop coefficient values in the conventional droop method are -0.003Ω, -0.006Ω and -0.009Ω. Also, -0.03Ω is intended for virtual resistance value. Figures 12 and 13 show the very long transient-state, very slow convergence and poor power sharing performance in the presence of uncertainties. According to detailed Tables I and II, it seems that the desirable performance of the proposed

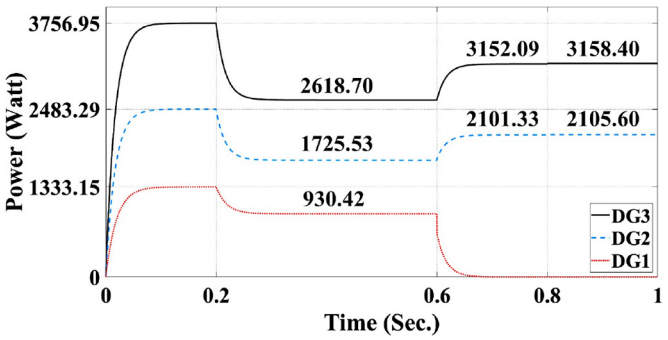

Fig. 12. The power sharing with the conventional droop control in Case 1.

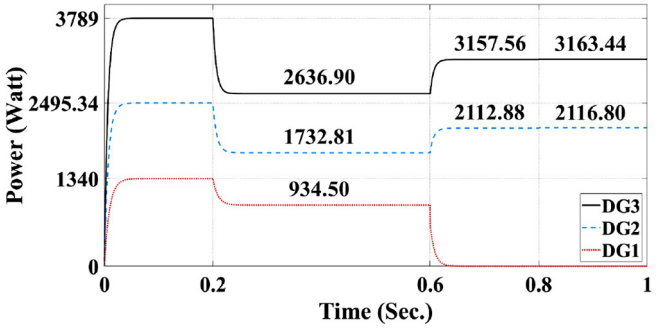

Fig. 13. The power sharing with the virtual resistance in Case 1.

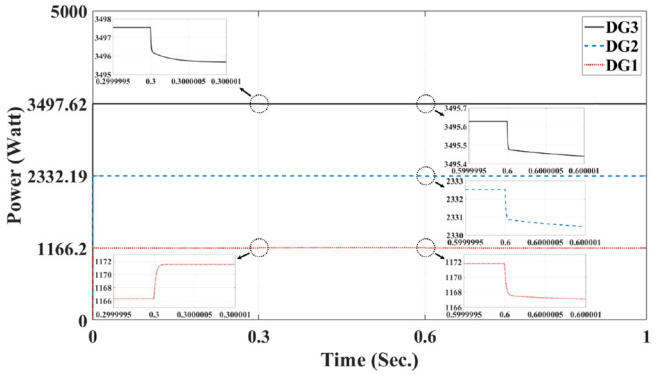

Fig. 14. The power sharing with the proposed DBSMC control in Case 2.

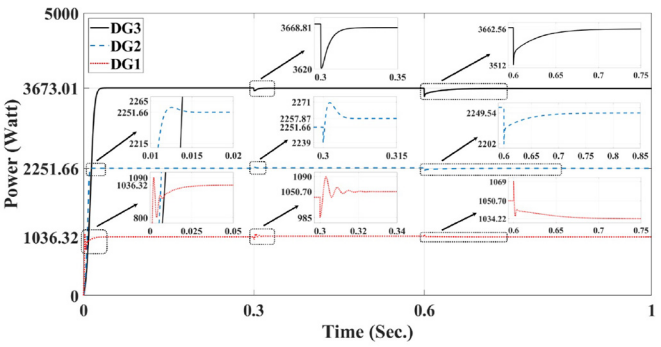

Fig. 15. The power sharing with the droop-based control [5] in Case 2.

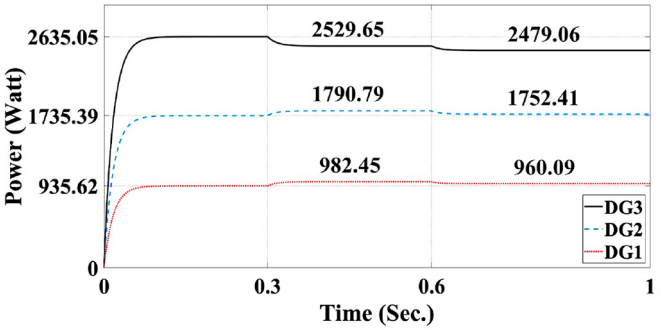

Fig. 16. The power sharing with the conventional droop control in Case 2.

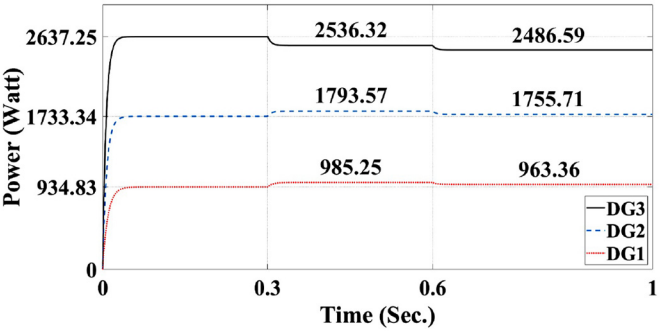

Fig. 17. The power sharing with the virtual resistance in Case 2.

DBSMC control in proportional power sharing can be concluded.

Case 2 (Changes of Line Resistances): The line resistance changes the total equivalent droop resistance. In this situation, the load sharing ratio will be different from the theoretical value. In practical applications, the droop controller capability to withstand possible changes in line resistance will be a privileged feature for the controller. To evaluate the proposed droop control capability, abrupt changes in line resistance are considered. For this purpose, the initial line resistances values 0.3Ω, 0.4Ω and 0.5Ω, while the load is 7kW, are suddenly changed. At 0.3s, the line resistances are changed to 0.2Ω, 0.4Ω and 0.6Ω, afterwards at 0.6s, the resistances are increased to 3 Ω, 2Ω and 1.5Ω; respectively.

Moreover, the parametric uncertainties and external disturbances are assumed as mentioned in Case 1. The droop-based FSMC control [5] is also implemented and simulated, under these challenging conditions. All of the control parameters, and bounds of the fuzzy approximator MFs, are mentioned and shown in Appendices D and E. Figures 14 and 15, demonstrate the results of the power sharing with the proposed droop control and the droop control [5]. Carefully in Figures 14 and 15 and considering detailed Table III, the robust and favorable performance of the proposed DBSMC control can be deduced. Also, the ratio of the power sharing with the proposed droop technique is closer to the ratio of DGs nominal power 1:2:3, compared to the droop control [5]. The results with the conventional droop control and with the virtual resistance compensation are shown in Figures 16 and 17. Considering detailed Tables III and IV, the favorable performance of the proposed DBSMC control in proportional power sharing is obvious.

Fig. 18. The used RTDS system.

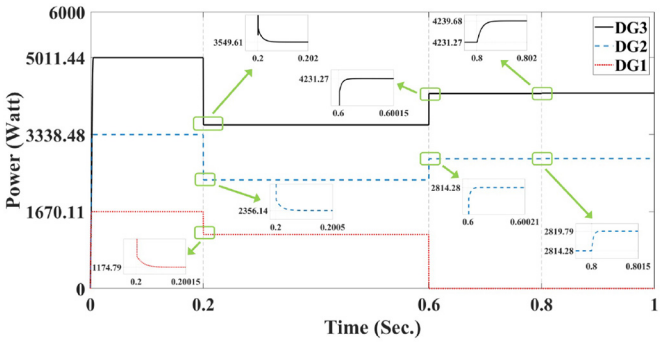

Fig. 19. The power sharing with the proposed DBSMC control in Case 1, in real-time digital simulation.

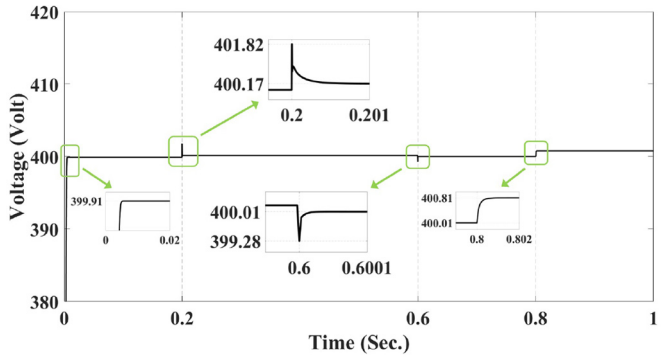

Fig. 20. The DC voltage with the proposed DBSMC control in Case 1, in real-time digital simulation.

B. Real-Time Digital Simulation Results

For evaluating the efficiency of the proposed DBSMC control strategy in the field of the isolated buck converter-based DC MG, the real-time digital simulation method is performed, using the RTDS system of Figure 18 consisting of five PB5 processing cards. The proposed DBSMC controller is exerted to the studied isolated DC MG in a real-time digital simulation, in varying operating conditions and in the presence of structured uncertainties and external disturbances, just like

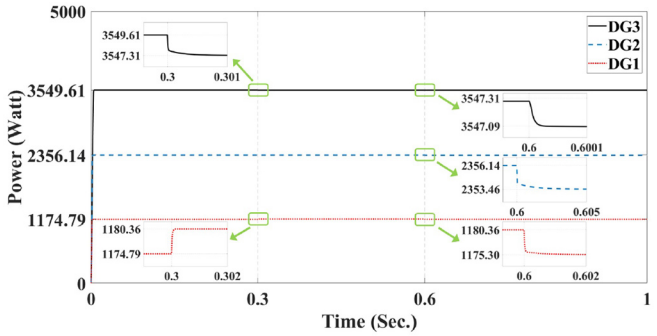

Fig. 21. The power sharing with the proposed DBSMC control in Case 2, in real-time digital simulation.

TABLE I
POWER SHARING WITH DROOP CONTROLLER [5] AND PROPOSED DBSMC CONTROLLER IN CASE 1

		With the droop controller [5]		With the proposed DBSMC controller			
		Output power (Watt)	Proportional Relation	Output power (Watt)		Proportional Relation	
				MATLAB	RTDS	MATLAB	RTDS
0S-0.2S	DG1	1510.43	0.9062	1669.94	1670.11	1.0020	1.0021
	DG2	3068.01	1.8408	3338.28	3338.48	2.0030	2.0031
	DG3	5276.05	3.1656	5011.07	5011.44	3.0066	3.0069
0.2S-0.6S	DG1	1036.32	0.8883	1166.20	1174.79	0.9996	1.0069
	DG2	2251.66	1.9299	2332.19	2356.14	1.9990	2.0195
	DG3	3673.01	3.1483	3497.62	3549.61	2.9980	3.0425
0.6S-0.8S	DG2	3096.36	2.2117	2799.07	2814.28	1.9993	2.0102
	DG3	3811.96	2.7228	4197.89	4231.27	2.9985	3.0223
0.8S-1S	DG2	3106.82	2.2191	2804.83	2819.79	2.0034	2.0141
	DG3	3813.50	2.7239	4205.64	4239.68	3.0040	3.0283

TABLE II
POWER SHARING WITH CONVENTIONAL DROOP CONTROL AND DROOP SCHEME WITH VIRTUAL RESISTANCE IN CASE 1

		With the conventional droop		With the virtual resistance	
		Output power (Watt)	Proportional Relation	Output Power (Watt)	Proportional Relation
0S-0.2S	DG1	1333.15	0.7998	1340.00	0.8040
	DG2	2483.29	1.4900	2495.34	1.4972
	DG3	3756.95	2.2542	3789.00	2.2734
0.2S-0.6S	DG1	930.42	0.7975	934.50	0.8010
	DG2	1725.53	1.4790	1732.81	1.4853
	DG3	2618.70	2.2446	2636.90	2.2602
0.6S-0.8S	DG2	2101.33	1.5009	2112.88	1.5092
	DG3	3152.09	2.2515	3157.56	2.2554
0.8S-1S	DG2	2105.60	1.5040	2116.80	1.5120
	DG3	3158.40	2.2560	3163.44	2.2596

Cases 1 and 2 and under the same conditions. About Case 1, with carefully in Figures 19 and 20, these favorable features can be seen; respectively: a) Very short transient-state and the fast convergence of the DGs output powers to the proportional power values, very close to the desired ratio of 1:2:3 and without considerable undershoot and/or overshoot, b) The precise voltage regulation. Also about Case 2, the robust and desired performance of the proposed DBSMC control is visible in Figure 21. As well as, the ratio of the power sharing with the proposed droop technique is close to the ratio of DGs nominal power 1:2:3. According to the detailed Tables I to IV, the favorable performance of the proposed DBSMC control in proportional power sharing, in Cases 1 and 2, can be deduced.

TABLE III
POWER SHARING WITH DROOP CONTROLLER [5] AND PROPOSED DBSMC CONTROLLER IN CASE 2

		With the droop controller [5]		With the proposed DBSMC controller			
		Output power (Watt)	Proportional Relation	Output power (Watt)		Proportional Relation	
				MATLAB	RTDS	MATLAB	RTDS
0S-0.3S	DG1	1036.32	0.8883	1166.20	1174.79	0.9996	1.0069
	DG2	2251.66	1.9299	2332.19	2356.14	1.9990	2.0195
	DG3	3673.01	3.1483	3497.62	3549.61	2.9980	3.0425
0.3S-0.6S	DG1	1050.70	0.9006	1171.68	1180.36	1.0043	1.0117
	DG2	2257.87	1.9353	2332.32	2356.14	1.9991	2.0195
	DG3	3668.81	3.1447	3495.63	3547.31	2.9963	3.0405
0.6S-1S	DG1	1034.22	0.8865	1167.38	1175.30	1.0006	1.0074
	DG2	2249.54	1.9282	2330.59	2353.46	1.9977	2.0172
	DG3	3662.56	3.1393	3495.45	3547.09	2.9961	3.0404

TABLE IV
POWER SHARING WITH CONVENTIONAL DROOP CONTROL AND DROOP SCHEME WITH VIRTUAL RESISTANCE IN CASE 2

		With the conventional droop		With the virtual resistance	
		Output power (Watt)	Proportional Relation	Output Power (Watt)	Proportional Relation
0S-0.3S	DG1	935.62	0.8019	934.83	0.8013
	DG2	1735.39	1.4875	1733.34	1.4857
	DG3	2635.05	2.2586	2637.25	2.2605
0.3S-0.6S	DG1	982.45	0.8421	985.25	0.8445
	DG2	1790.79	1.5350	1793.57	1.5373
	DG3	2529.65	2.1683	2536.32	2.1740
0.6S-1S	DG1	960.09	0.8230	963.36	0.8257
	DG2	1752.41	1.5021	1755.71	1.5049
	DG3	2479.06	2.1250	2486.59	2.1314

VI. CONCLUSION

In this paper, a novel nonlinear robust droop control strategy is proposed for proportional, accurate and fast power sharing of isolated DC MG, with an improved nonlinear droop model, in the presence of variable operating conditions, structured uncertainties and external disturbances. The controller designing is based on the sliding mode approach and a fuzzy approximation technique. The proposed DBSMC control strategy is a decentralized control without the need for any communication links. The low computing volume of the control input as well as the simplicity and step-by-step nature of the controller design process, increase the proposed controller's ability to implement in practice. The simulation results achieved from the MATLAB software also real-time simulation results from an RTDS system represented the desirable performance of the proposed DBSMC controller.

APPENDIX A
THE VECTOR $f(x)$ IS AS FOLLOWS

Equation shown at the bottom of the next page.

APPENDIX B
THE PROOF OF THEOREM 1

Proof: sliding surface S is considered as the sum of sliding surfaces s_1 and s_2:

$$S = s_1 + s_2 \tag{B.1}$$

To design the control input $u_s(t)$, the following Lyapunov candidate function is proposed:

$$V(S) = \frac{1}{2}S^2 \tag{B.2}$$

Differentiating with respect to time in the equation (B.2) we obtain:

$$\dot{V}(S) = S\dot{S} = S[\xi\dot{e}_1 + \zeta\dot{e}_6] \tag{B.3}$$

Due to the remark 3, (20), (23) and (24) are placed in (B.3):

$$\begin{aligned}
\dot{V}(S) &= S\dot{S} \\
&= S\left\{ \begin{matrix} \xi\begin{pmatrix} f_{c1} + g_{c1}u(t) \\ +D_1(t) - \dot{x}_{d1} \end{pmatrix} \\ \zeta\begin{pmatrix} f_{c2} + g_{c2}u(t) \\ +D_2(t) - \dot{x}_{d6} \end{pmatrix} \end{matrix} \right\} \\
&= S\left\{ \begin{matrix} \xi\left(f_{c1} + g_{c1}\begin{pmatrix} u_{eq1}(t) \\ +u_{eq2}(t) \\ +u_s(t) \end{pmatrix} \right) \\ +D_1(t) - \dot{x}_{d1} \\ +\zeta\left(f_{c2} + g_{c2}\begin{pmatrix} u_{eq1}(t) \\ +u_{eq2}(t) \\ +u_s(t) \end{pmatrix} \right) \\ +D_2(t) - \dot{x}_{d6} \end{matrix} \right\} \\
&= S\left\{ \begin{matrix} \xi f_{c1} + \xi g_{c1}u_{eq1}(t) + \xi g_{c1}u_{eq2}(t) + \xi g_{c1}u_s(t) \\ +\xi D_1(t) - \xi\dot{x}_{d1} + \\ \zeta f_{c2} + \zeta g_{c2}u_{eq1}(t) + \zeta g_{c2}u_{eq2}(t) + \zeta g_{c2}u_s(t) \\ +\zeta D_2(t) - \zeta\dot{x}_{d6} \end{matrix} \right\} \\
&= S\left\{ \begin{matrix} \big(\xi g_{c1} + \zeta g_{c2}\big)\big(u_{eq1}(t) + u_{eq2}(t)\big) \\ + \big(\xi g_{c1} + \zeta g_{c2}\big)u_s(t) + \xi f_{c1} + \zeta f_{c2} \\ + \xi D_1(t) + \zeta D_2(t) - \xi\dot{x}_{d1} - \zeta\dot{x}_{d6} \end{matrix} \right\}
\end{aligned} \tag{B.4}$$

The control input $u_s(t)$ is selected as follows:

$$u_s(t) = \frac{-1}{\left\{ \begin{matrix} \xi g_{c1} \\ +\zeta g_{c2} \end{matrix} \right\}} \left\{ \begin{matrix} \big(\xi g_{c1} + \zeta g_{c2}\big)\begin{pmatrix} u_{eq1}(t) \\ +u_{eq2}(t) \end{pmatrix} \\ +\xi f_{c1} + \zeta f_{c2} - (\xi\dot{x}_{d1} + \zeta\dot{x}_{d6}) \\ +kS + \rho sat(S) \end{matrix} \right\} \tag{B.5}$$

where k and ρ are positive constants. The function $sat(S)$ is defined as:

$$sat(S) = \begin{cases} sgn(S), & |S| > \varepsilon \\ S/\varepsilon, & |S| \le \varepsilon \end{cases} \tag{B.6}$$

where $sgn(S)$ is equal to $\frac{S}{|S|}$ and ε is a small positive constant.

By placing (B.5) in (B.4) and considering (B.6) we have:

$$\begin{aligned}
\dot{V}(S) = S\dot{S} &= S\left\{ \begin{matrix} -kS - \rho sat(S) \\ +\xi D_1(t) + \zeta D_2(t) \end{matrix} \right\} \\
&= -kS^2 - \rho S sat(S) + S(\xi D_1(t) + \zeta D_2(t)) \\
&\le -\rho S sat(S) + \big(\xi D_1^{\max} + \zeta D_2^{\max}\big) S sat(S) \\
&= \begin{cases} \big(-\rho + \big(\xi D_1^{\max} + \zeta D_2^{\max}\big)\big)|S|, & |S| > \varepsilon \\ \big(-\rho + \big(\xi D_1^{\max} + \zeta D_2^{\max}\big)\big)\frac{S^2}{\varepsilon}, & |S| \le \varepsilon \end{cases}
\end{aligned} \tag{B.7}$$

From (B.7) it follows that by properly selecting the coefficients ξ, ζ, ε, k and ρ and satisfying the condition $\rho > (\xi D_1^{\max} + \zeta D_2^{\max})$ derivative of Lyapunov function becomes less than zero. Therefore, over time, the sliding surface S converges to zero. ■

Remark 7: Although with proper selection of coefficients ξ, ζ, ε, k and ρ, the convergence of sliding surface S to zero can be deduced from (B.7), but it is not necessarily possible to conclude zero sliding surfaces s_1 and s_2 by zeroing the sliding

surface S. Therefore, zero sliding surface S does not guarantee the stability of the closed-loop system (20).

It has been proved so far that the control input expressed in (23) and (24) converges the sliding surface S to zero in the presence of existing structured uncertainties and external disturbances. Next, it will be proved that zeroing the sliding surface S causes zero sliding surfaces s_1 and s_2. Finally, the closed-loop system (20) will have global asymptotic stability, and Theorem 1 will be proved. To analyze the stability of the system (20), we first take the integral from both sides of the first part of (B.7) with respect to time:

$$\int_0^t \dot{V}dt = \int_0^t \left(-\rho|S| + |S|\left(\xi D_1^{\max} + \zeta D_2^{\max}\right)\right)dt$$
$$V(t) - V(0) = \int_0^t \left(-\left(\rho - \left(\xi D_1^{\max} + \zeta D_2^{\max}\right)\right)|S|\right)dt \quad \text{(B.8)}$$

From (B.2) and (22) we have:

$$V(t) = \frac{1}{2}S^2 = V(0) - \int_0^\infty \left(\left(\rho - \left(\xi D_1^{\max} + \zeta D_2^{\max}\right)\right)|S|\right)dt \le V(0) < \infty \quad \text{(B.9)}$$

$$\begin{bmatrix}
-\omega_c\Delta P + \omega_c I_{op}\Delta V_o;\ \sqrt{\frac{\Delta P}{K_d} + 0.25V_{op}^2} - 0.5V_{op} - \Delta V_o;\\
K_{Iv}\Delta\Psi - \Delta I_{dg} - K_{Pv}\Delta V_o + K_{Pv}\left(\sqrt{\frac{\Delta P}{K_d} + 0.25V_{op}^2} - 0.5V_{op}\right);\\
K_{Ii}\left(V_{E_n} + \Delta V_E\right)\Delta\Gamma/L + K_{Pi}K_{Iv}\left(V_{E_n} + \Delta V_E\right)\Delta\Psi/L + K_{Pi}K_{Pv}\left(\sqrt{\frac{\Delta P}{K_d} + 0.25V_{op}^2} - 0.5V_{op}\right)\left(V_{E_n} + \Delta V_E\right)/L\\
\quad - K_{Pi}K_{Pv}\left(V_{E_n} + \Delta V_E\right)\Delta V_o/L - K_{Pi}\left(V_{E_n} + \Delta V_E\right)\Delta I_{dg}/L - K_{Ii}\left(R_{dg}\Delta I_{dg} + R_L I_{RL}\right)\Delta\Gamma/L\\
\quad - K_{Pi}K_{Iv}\left(R_{dg}\Delta I_{dg} + R_L I_{RL}\right)\Delta\Psi/L - K_{Pi}K_{Pv}\left(\sqrt{\frac{\Delta P}{K_d} + 0.25V_{op}^2} - 0.5V_{op}\right)\left(R_{dg}\Delta I_{dg} + R_L I_{RL}\right)/L\\
\quad + K_{Pi}K_{Pv}\left(R_{dg}\Delta I_{dg} + R_L I_{RL}\right)\Delta V_o/L + K_{Pi}\left(R_{dg}\Delta I_{dg} + R_L I_{RL}\right)\Delta I_{dg}/L - \left(V_{op} + \Delta V_o\right)/L;\\
K_{Ii}^2\left(V_{E_n} + \Delta V_E\right)(\Delta\Gamma)^2/L + K_{Pi}K_{Iv}K_{Ii}\left(V_{E_n} + \Delta V_E\right)\Delta\Gamma\Delta\Psi/L + K_{Pi}K_{Pv}K_{Ii}\left(\sqrt{\frac{\Delta P}{K_d} + 0.25V_{op}^2} - 0.5V_{op}\right)\left(V_{E_n} + \Delta V_E\right)\Delta\Gamma/L\\
\quad - K_{Pi}K_{Pv}K_{Ii}\left(V_{E_n} + \Delta V_E\right)\Delta\Gamma\Delta V_o/L - K_{Pi}K_{Ii}\left(V_{E_n} + \Delta V_E\right)\Delta\Gamma\Delta I_{dg}/L - K_{Ii}^2\left(R_{dg}\Delta I_{dg} + R_L I_{RL}\right)(\Delta\Gamma)^2/L\\
\quad - K_{Pi}K_{Iv}K_{Ii}\left(R_{dg}\Delta I_{dg} + R_L I_{RL}\right)\Delta\Gamma\Delta\Psi/L - K_{Pi}K_{Pv}K_{Ii}\left(\sqrt{\frac{\Delta P}{K_d} + 0.25V_{op}^2} - 0.5V_{op}\right)\left(R_{dg}\Delta I_{dg} + R_L I_{RL}\right)\Delta\Gamma/L\\
\quad + K_{Pi}K_{Pv}K_{Ii}\left(R_{dg}\Delta I_{dg} + R_L I_{RL}\right)\Delta\Gamma\Delta V_o/L + K_{Pi}K_{Ii}\left(R_{dg}\Delta I_{dg} + R_L I_{RL}\right)\Delta\Gamma\Delta I_{dg}/L - K_{Ii}\left(V_{op} + \Delta V_o\right)\Delta\Gamma/L\\
\quad + K_{Pi}K_{Iv}K_{Ii}\left(V_{E_n} + \Delta V_E\right)\Delta\Gamma\Delta\Psi/L + K_{Pi}^2K_{Iv}^2\left(V_{E_n} + \Delta V_E\right)(\Delta\Psi)^2/L + K_{Pi}^2K_{Pv}K_{Iv}\left(\sqrt{\frac{\Delta P}{K_d} + 0.25V_{op}^2} - 0.5V_{op}\right)\\
\quad \times \left(V_{E_n} + \Delta V_E\right)\Delta\Psi/L - K_{Pi}^2K_{Pv}K_{Iv}\left(V_{E_n} + \Delta V_E\right)\Delta\Psi\Delta V_o/L - K_{Pi}^2K_{Iv}\left(V_{E_n} + \Delta V_E\right)\Delta\Psi\Delta I_{dg}/L\\
\quad - K_{Pi}K_{Iv}K_{Ii}\left(R_{dg}\Delta I_{dg} + R_L I_{RL}\right)\Delta\Gamma\Delta\Psi/L - K_{Pi}^2K_{Iv}^2\left(R_{dg}\Delta I_{dg} + R_L I_{RL}\right)(\Delta\Psi)^2/L - K_{Pi}^2K_{Pv}K_{Iv}\left(\sqrt{\frac{\Delta P}{K_d} + 0.25V_{op}^2} - 0.5V_{op}\right)\\
\quad \times \left(R_{dg}\Delta I_{dg} + R_L I_{RL}\right)\Delta\Psi/L + K_{Pi}^2K_{Pv}K_{Iv}\left(R_{dg}\Delta I_{dg} + R_L I_{RL}\right)\Delta\Psi\Delta V_o/L + K_{Pi}^2K_{Iv}\left(R_{dg}\Delta I_{dg} + R_L I_{RL}\right)\Delta I_{dg}\Delta\Psi/L\\
\quad - K_{Pi}K_{Iv}\left(V_{op} + \Delta V_o\right)\Delta\Psi/L + K_{Pi}K_{Pv}K_{Ii}\left(\sqrt{\frac{\Delta P}{K_d} + 0.25V_{op}^2} - 0.5V_{op}\right)\left(V_{E_n} + \Delta V_E\right)\Delta\Gamma/L + K_{Pi}^2K_{Pv}K_{Iv}\\
\quad \times \left(\sqrt{\frac{\Delta P}{K_d} + 0.25V_{op}^2} - 0.5V_{op}\right)\left(V_{E_n} + \Delta V_E\right)\Delta\Psi/L + K_{Pi}^2K_{Pv}^2\left(\sqrt{\frac{\Delta P}{K_d} + 0.25V_{op}^2} - 0.5V_{op}\right)^2\left(V_{E_n} + \Delta V_E\right)/L\\
\quad - K_{Pi}^2K_{Pv}^2\left(\sqrt{\frac{\Delta P}{K_d} + 0.25V_{op}^2} - 0.5V_{op}\right)\left(V_{E_n} + \Delta V_E\right)\Delta V_o/L - K_{Pi}^2K_{Pv}\left(\sqrt{\frac{\Delta P}{K_d} + 0.25V_{op}^2} - 0.5V_{op}\right)\left(V_{E_n} + \Delta V_E\right)\Delta I_{dg}/L\\
\quad - K_{Pi}K_{Pv}K_{Ii}\left(\sqrt{\frac{\Delta P}{K_d} + 0.25V_{op}^2} - 0.5V_{op}\right)\left(R_{dg}\Delta I_{dg} + R_L I_{RL}\right)\Delta\Gamma/L - K_{Pi}^2K_{Pv}K_{Iv}\left(\sqrt{\frac{\Delta P}{K_d} + 0.25V_{op}^2} - 0.5V_{op}\right)\\
\quad \times \left(R_{dg}\Delta I_{dg} + R_L I_{RL}\right)\Delta\Psi/L - K_{Pi}^2K_{Pv}^2\left(\sqrt{\frac{\Delta P}{K_d} + 0.25V_{op}^2} - 0.5V_{op}\right)^2\left(R_{dg}\Delta I_{dg} + R_L I_{RL}\right)/L\\
\quad + K_{Pi}^2K_{Pv}^2\left(\sqrt{\frac{\Delta P}{K_d} + 0.25V_{op}^2} - 0.5V_{op}\right)\left(R_{dg}\Delta I_{dg} + R_L I_{RL}\right)\Delta V_o/L + K_{Pi}^2K_{Pv}\left(\sqrt{\frac{\Delta P}{K_d} + 0.25V_{op}^2} - 0.5V_{op}\right)\\
\quad \times \left(R_{dg}\Delta I_{dg} + R_L I_{RL}\right)\Delta I_{dg}/L - K_{Pi}K_{Pv}\left(\sqrt{\frac{\Delta P}{K_d} + 0.25V_{op}^2} - 0.5V_{op}\right)\left(V_{op} + \Delta V_o\right)/L - K_{Pi}K_{Pv}K_{Ii}\left(V_{E_n} + \Delta V_E\right)\Delta\Gamma\Delta V_o/L\\
\quad - K_{Pi}^2K_{Pv}K_{Iv}\left(V_{E_n} + \Delta V_E\right)\Delta\Psi\Delta V_o/L - K_{Pi}^2K_{Pv}^2\left(\sqrt{\frac{\Delta P}{K_d} + 0.25V_{op}^2} - 0.5V_{op}\right)\left(V_{E_n} + \Delta V_E\right)\Delta V_o/L\\
\quad + K_{Pi}^2K_{Pv}^2\left(V_{E_n} + \Delta V_E\right)(\Delta V_o)^2/L + K_{Pi}^2K_{Pv}\left(V_{E_n} + \Delta V_E\right)\Delta I_{dg}\Delta V_o/L + K_{Pi}K_{Pv}K_{Ii}\left(R_{dg}\Delta I_{dg} + R_L I_{RL}\right)\Delta\Gamma\Delta V_o/L\\
\quad + K_{Pi}^2K_{Pv}K_{Iv}\left(R_{dg}\Delta I_{dg} + R_L I_{RL}\right)\Delta\Psi\Delta V_o/L + K_{Pi}^2K_{Pv}^2\left(\sqrt{\frac{\Delta P}{K_d} + 0.25V_{op}^2} - 0.5V_{op}\right)\left(R_{dg}\Delta I_{dg} + R_L I_{RL}\right)\Delta V_o/L\\
\quad - K_{Pi}^2K_{Pv}^2\left(R_{dg}\Delta I_{dg} + R_L I_{RL}\right)(\Delta V_o)^2/L - K_{Pi}^2K_{Pv}\left(R_{dg}\Delta I_{dg} + R_L I_{RL}\right)\Delta I_{dg}\Delta V_o/L + K_{Pi}K_{Pv}\left(V_{op} + \Delta V_o\right)\Delta V_o/L\\
\quad - K_{Pi}K_{Ii}\left(V_{E_n} + \Delta V_E\right)\Delta\Gamma\Delta I_{dg}/L - K_{Pi}^2K_{Iv}\left(V_{E_n} + \Delta V_E\right)\Delta\Psi\Delta I_{dg}/L - K_{Pi}^2K_{Pv}\left(\sqrt{\frac{\Delta P}{K_d} + 0.25V_{op}^2} - 0.5V_{op}\right)\\
\quad \times \left(V_{E_n} + \Delta V_E\right)\Delta I_{dg}/L + K_{Pi}^2K_{Pv}\left(V_{E_n} + \Delta V_E\right)\Delta I_{dg}\Delta V_o/L + K_{Pi}^2\left(V_{E_n} + \Delta V_E\right)\left(\Delta I_{dg}\right)^2/L + K_{Pi}K_{Ii}\left(R_{dg}\Delta I_{dg} + R_L I_{RL}\right)\\
\quad \times \Delta\Gamma\Delta I_{dg}/L + K_{Pi}^2K_{Iv}\left(R_{dg}\Delta I_{dg} + R_L I_{RL}\right)\Delta\Psi\Delta I_{dg}/L + K_{Pi}^2K_{Pv}\left(\sqrt{\frac{\Delta P}{K_d} + 0.25V_{op}^2} - 0.5V_{op}\right)\left(R_{dg}\Delta I_{dg} + R_L I_{RL}\right)\Delta I_{dg}/L\\
\quad - K_{Pi}^2K_{Pv}\left(R_{dg}\Delta I_{dg} + R_L I_{RL}\right)\Delta I_{dg}\Delta V_o/L - K_{Pi}^2\left(R_{dg}\Delta I_{dg} + R_L I_{RL}\right)\left(\Delta I_{dg}\right)^2/L + K_{Pi}\left(V_{op} + \Delta V_o\right)\Delta I_{dg}/L;\\
K_{Ii}\left(\Delta I_{dg} + I_{RL}\right)\Delta\Gamma/C + K_{Pi}K_{Iv}\left(\Delta I_{dg} + I_{RL}\right)\Delta\Psi/C + K_{Pi}K_{Pv}\left(\sqrt{\frac{\Delta P}{K_d} + 0.25V_{op}^2} - 0.5V_{op}\right)\left(\Delta I_{dg} + I_{RL}\right)/C\\
\quad - K_{Pi}K_{Pv}\left(\Delta I_{dg} + I_{RL}\right)\Delta V_o/C - K_{Pi}\left(\Delta I_{dg} + I_{RL}\right)\Delta I_{dg}/C - K_{Ii}(\Delta I_L + I_{RL})\Delta\Gamma/C - K_{Pi}K_{Iv}(\Delta I_L + I_{RL})\Delta\Psi/C\\
\quad - K_{Pi}K_{Pv}\left(\sqrt{\frac{\Delta P}{K_d} + 0.25V_{op}^2} - 0.5V_{op}\right)(\Delta I_L + I_{RL})/C + K_{Pi}K_{Pv}(\Delta I_L + I_{RL})\Delta V_o/C\\
\quad + K_{Pi}(\Delta I_L + I_{RL})\Delta I_{dg}/C + (\Delta I_L + I_{RL})/C - I_{op}/C;
\end{bmatrix}$$

From (B.9) it follows that $S \in L_\infty$:

$$\sup_{t\geq 0}|S| = \|S\|_\infty < \infty \tag{B.10}$$

From (B.7) and (B.10) we have:

$$\dot{V}(S) = S\dot{S} \leq -\rho|S| + |S|\left(\xi D_1^{\max} + \zeta D_2^{\max}\right) < \infty \tag{B.11}$$

From (B.11) it results that $\dot{S} \in L_\infty$:

$$\sup_{t\geq 0}|\dot{S}| = \|\dot{S}\|_\infty < \infty \tag{B.12}$$

Therefore, from (B.10) and (B.12) it can be concluded that:

$$\begin{cases} \sup\limits_{t\geq 0}|s_1| = \|s_1\|_\infty < \infty \\ \sup\limits_{t\geq 0}|\dot{s}_1| = \|\dot{s}_1\|_\infty < \infty \end{cases}; \quad \begin{cases} \sup\limits_{t\geq 0}|s_2| = \|s_2\|_\infty < \infty \\ \sup\limits_{t\geq 0}|\dot{s}_2| = \|\dot{s}_2\|_\infty < \infty \end{cases} \tag{B.13}$$

In the light of the above description, we know that if $\rho > (\xi D_1^{\max} + \zeta D_2^{\max})$, then the values of ξ and ζ have not a direct effect on the system stability. Therefore, the following two sliding surfaces are introduced:

$$\begin{cases} S_1 = \xi_1 s_1 + \zeta s_2 \\ S_2 = \xi_2 s_1 + \zeta s_2 \end{cases} \tag{B.14}$$

where ξ_1 and ξ_2 are arbitrary constants and $\xi_1 \neq \xi_2$, so $S_1 \neq S_2$. Also $0 < \int_0^\infty S_2^2 dt < \int_0^\infty S_1^2 dt < \infty$ is assumed. From (B.9) we have:

$$\begin{cases} 0 \leq \int_0^\infty S_1^2 dt < \int_0^\infty \left(\xi_1^2 s_1^2 + 2\xi_1\zeta s_1 s_2 + \zeta^2 s_2^2\right) dt < \infty \\ 0 \leq \int_0^\infty S_2^2 dt < \int_0^\infty \left(\xi_2^2 s_1^2 + 2\xi_2\zeta s_1 s_2 + \zeta^2 s_2^2\right) dt < \infty \end{cases} \tag{B.15}$$

So we have:

$$\begin{aligned} 0 &< \int_0^\infty \left(S_1^2 - S_2^2\right) dt \\ &= \int_0^\infty \left(\left(\xi_1^2 - \xi_2^2\right) s_1^2 + 2(\xi_1 - \xi_2)\zeta s_1 s_2\right) dt < \infty \end{aligned} \tag{B.16}$$

The above relation is rewritten in terms of s_1 and S_1:

$$\begin{aligned} &\int_0^\infty \left(\left(\xi_1^2 - \xi_2^2\right) s_1^2 + 2(\xi_1 - \xi_2) s_1 (S_1 - \xi_1 s_1)\right) dt \\ &= \int_0^\infty -(\xi_1 - \xi_2)^2 s_1^2 dt + \int_0^\infty 2(\xi_1 - \xi_2) s_1 S_1 dt > 0 \end{aligned} \tag{B.17}$$

From (B.9) can be concluded:

$$\int_0^\infty \left(\rho - \left(\xi D_1^{\max} + \zeta D_2^{\max}\right)\right)|S| dt \leq V(0) < \infty \tag{B.18}$$

Since $\rho > (\xi D_1^{\max} + \zeta D_2^{\max})$, so: $\int_0^\infty (\rho - (\xi D_1^{\max} + \zeta D_2^{\max}))|S| dt \geq 0$. This positive value will be limited. So it can be concluded that: $0 \leq (\rho - (\xi D_1^{\max} + \zeta D_2^{\max})) \int_0^\infty |S| dt = \|S\|_1 \leq \infty$.

Hence $S \in L_1$. In the following, from (B.17) we get:

$$\begin{aligned} &\int_0^\infty (\xi_1 - \xi_2)^2 s_1^2 dt < \int_0^\infty 2(\xi_1 - \xi_2) s_1 S_1 dt \\ &\leq 2\int_0^\infty |(\xi_1 - \xi_2) s_1 S_1| dt \leq 2|\xi_1 - \xi_2| \int_0^\infty \|s_1\|_\infty |S_1| dt \\ &= 2|\xi_1 - \xi_2| \|s_1\|_\infty \|S_1\|_1 < \infty \end{aligned} \tag{B.19}$$

From (B.19) we have:

$$\int_0^\infty s_1^2 dt < \infty \tag{B.20}$$

TABLE V
IMPROVED DROOP MODEL PARAMETERS

Symbol	Description	DG	Values
C	Output capacitance of the converter (μF)	DG1, DG2, DG3	3.5, 6.5, 9.5
L	Inductor of the converter (μH)	DG1, DG2, DG3	2200, 1100, 800
R_{dg}	The internal resistance of the converter (Ω)	DG1, DG2, DG3	48, 24, 16
$k_{d_{initial}}$	Initial droop coefficient	DG1, DG2, DG3	-0.6, -1.2, -1.8
K_{Pv}	The ratio coefficient of the PI voltage controller	DG1, DG2, DG3	0.0802, 0.15643, 0.2338
K_{Iv}	The integral coefficient of the PI voltage controller	DG1, DG2, DG3	0.0001, 0.0001, 0.0001
K_{Pi}	The ratio coefficient of the PI current controller	DG1, DG2, DG3	105, 105.5, 106
K_{Ii}	The integral coefficient of the PI current controller	DG1, DG2, DG3	0.25, 0.252, 0.26

TABLE VI
THE PARAMETERS OF THE TRIPLE DBSMC CONTROLLERS

Symbol	Description	DBSMC Controller	Values	
			Case1	Case2
k	Control parameter	SMC1	5	5
		SMC2	10	10
		SMC3	15	15
ρ	Control parameter	SMC1	30	130
		SMC2	32	160
		SMC3	53	920
ε	Thickness of the boundary layer	SMC1	0.01	0.01
		SMC2	0.01	0.01
		SMC3	0.01	0.01
$d_1^{\max}$	The upper bound of applied external disturbance to state variable ΔP (W)	SMC1	30	30
		SMC2	60	60
		SMC3	90	90
$d_2^{\max}$	The upper bound of applied external disturbance to state variable ΔV_o (V)	SMC1	2	2
		SMC2	2	2
		SMC3	2	2

It is proved in a similar way that:

$$\int_0^\infty s_2^2 dt < \infty \tag{B.21}$$

From (B.20) and (B.21) it can be concluded that $s_1 \in L_2$ and $s_2 \in L_2$. Since $s_1 \in L_\infty$, $\dot{s}_1 \in L_\infty$, $s_2 \in L_\infty$ and $\dot{s}_2 \in L_\infty$, therefore, it can be deduced that $\lim_{t\to\infty} s_1 = 0$ and $\lim_{t\to\infty} s_2 = 0$, based on Barbalat's lemma [27], and Theorem 1 is proved. Similarly, for the second part of (B.7), Theorem 1 can be proved.

APPENDIX C
THE IMPROVED DROOP MODEL PARAMETERS

See Table V.

APPENDIX D
THE PARAMETERS OF THE TRIPLE DBSMC CONTROLLERS AND BOUNDS OF THE FUZZY APPROXIMATOR MFS

See Table VI and Table VII.

APPENDIX E
THE FUZZY APPROXIMATED DBSMC CONTROL PARAMETERS

Remark 8: According to advantage 3, expressed in Section IV-B, quick approximation of the control parameters ξ and ζ is obvious.

TABLE VII
BOUNDS OF THE FUZZY APPROXIMATOR MFS

			MFs Bounds for SMC1	MFs Bounds for SMC2	MFs Bounds for SMC3
$\frac{\Delta TEEC_\xi}{\Delta \xi}$	A	Case1	2.5	17	15
		Case2	0.4	0.5	0.2
$\Delta \xi$	B	Case1	0.5	0.1	0.1
		Case2	3.5	2.2	10
$\frac{\Delta TEEC_\zeta}{\Delta \zeta}$	A	Case1	1.1	1.5	1.5
		Case2	0.8	8	10
$\Delta \zeta$	B	Case1	1	0.7	0.8
		Case2	1.5	0.2	0.1

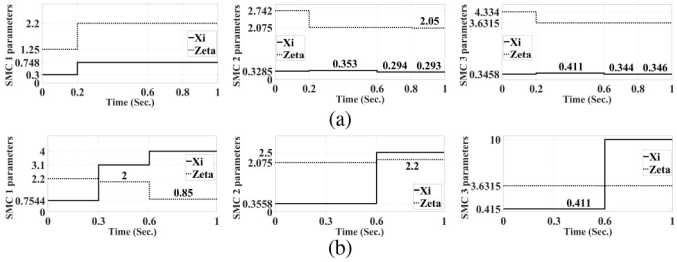

Fig. 22. Fuzzy approximated SMC control parameters (a) Case 1 (b) Case 2.

REFERENCES

[1] M. Lexuan *et al.*, "Review on control of DC microgrids and multiple microgrid clusters," *IEEE J. Emerg. Sel. Topics Power Electron.*, vol. 5, no. 3, pp. 928–948, Sep. 2017.

[2] A. T. Elsayed, A. A. Mohamed, and O. A. Mohammed, "DC microgrids and distribution systems: An overview," *Electr. Power Syst. Res.*, vol. 119, no. 1, pp. 407–417, Feb. 2015.

[3] J. J. Justo, F. Mwasilu, J. Lee, and J.-W. Jung, "AC-microgrids versus DC-microgrids with distributed energy resources: A review," *Renew. Sustain. Energy Rev.*, vol. 24, no. 1, pp. 387–405, Aug. 2013.

[4] T. Dragičević, X. Lu, J. C. Vasquez, and J. M. Guerrero, "DC microgrids—Part I: A review of control strategies and stabilization techniques," *IEEE Trans. Power Electron.*, vol. 31, no. 7, pp. 4876–4891, Jul. 2016.

[5] Y. Mi, H. Zhang, Y. Fu, C. Wang, P. C. Loh, and P. Wang, "Intelligent power sharing of DC isolated microgrid based on fuzzy sliding mode droop control," *IEEE Trans. Smart Grid*, vol. 10, no. 3, pp. 2396–2406, May 2019.

[6] F. Chen, R. Burgos, D. Boroyevich, and W. Zhang, "A nonlinear droop method to improve voltage regulation and load sharing in DC systems," in *Proc. IEEE 1st Int. Conf. DC Microgrids (ICDCM)*, 2015, pp. 45–50.

[7] P.-H. Huang, P.-C. Liu, W. Xiao, and M. S. El Moursi, "A novel droop-based average voltage sharing control strategy for DC microgrids," *IEEE Trans. Smart Grid*, vol. 6, no. 3, pp. 1096–1106, May 2015.

[8] A. Khorsandi, M. Ashourloo, H. Mokhtari, and R. Iravani, "Automatic droop control for a low voltage DC microgrid," *IET Gener. Transm. Distrib.*, vol. 10, no. 1, pp. 41–47, Jan. 2016.

[9] C. Dou, Z. Zhang, D. Yue, and M. Song, "Improved droop control based on virtual impedance and virtual power source in low-voltage microgrid," *IET Gener. Transm. Distrib.*, vol. 11, no. 4, pp. 1046–1054, Mar. 2017.

[10] H. Moussa, A. Shahin, J. P. Martin, S. Pierfederici, and N. Moubayed, "Optimal angle droop for power sharing enhancement with stability improvement in islanded microgrids," *IEEE Trans. Smart Grid*, vol. 9, no. 5, pp. 5014–5026, Sep. 2018.

[11] F. Chen, W. Zhang, R. Burgos, and D. Boroyevich, "Droop voltage range design in DC micro-grids considering cable resistance," in *Proc. IEEE Energy Convers. Congr. Exposit. (ECCE)*, 2014, pp. 770–777.

[12] R. Majumder, B. Chaudhuri, A. Ghosh, R. Majumder, G. Ledwich, and F. Zare, "Improvement of stability and load sharing in an autonomous microgrid using supplementary droop control loop," *IEEE Trans. Power Syst.*, vol. 25, no. 2, pp. 796–808, May 2010.

[13] J. He and Y. W. Li, "An enhanced microgrid load demand sharing strategy," *IEEE Trans. Power Electron.*, vol. 27, no. 9, pp. 3984–3995, Sep. 2012.

[14] J. Mohammadi and F. B. Ajaei, "Improved mode-adaptive droop control strategy for the DC microgrid," *IEEE Access*, vol. 7, pp. 86421–86435, 2019.

[15] V. Nasirian, A. Davoudi, and F. L. Lewis, "Distributed adaptive droop control for DC microgrids," in *Proc. IEEE Appl. Power Electron. Conf. Exposit.*, 2014, pp. 1147–1152.

[16] S. Augustine, M. K. Mishra, and N. Lakshminarasamma, "Adaptive droop control strategy for load sharing and circulating current minimization in low-voltage standalone DC microgrid," *IEEE Trans. Sustain. Energy*, vol. 6, no. 1, pp. 132–141, Jan. 2015.

[17] C. A. Macana, E. Mojica-Nava, H. R. Pota, J. Guerrero, and J. C. Vasquez, "Accurate proportional power sharing with minimum communication requirements for inverter-based islanded microgrids," *Int. J. Electr. Power Energy Syst.*, vol. 121, no. 1, Oct. 2020, Art. no. 106036.

[18] M. Baharizadeh, M. S. Golsorkhi, M. Shahparasti, and M. Savaghebi, "A two-layer control scheme based on $P-V$ droop characteristic for accurate power sharing and voltage regulation in DC microgrids," *IEEE Trans. Smart Grid*, vol. 12, no. 4, pp. 2776–2787, Jul. 2021.

[19] Y. Mi *et al.*, "A power sharing strategy for islanded DC microgrid with unmatched line impedance and local load," *Electr. Power Syst. Res.*, vol. 192, no. 1, Mar. 2021, Art. no. 106983.

[20] S. Peyghami, P. Davari, H. Mokhtari, and F. Blaabjerg, "Decentralized droop control in DC microgrids based on a frequency injection approach," *IEEE Trans. Smart Grid*, vol. 10, no. 6, pp. 6782–6791, Nov. 2019.

[21] H. Yang, X. Ning, L. Li, P. Yang, and F. Blaabjerg, "Droop coefficient correction control for power sharing and voltage restoration in hierarchical controlled DC microgrids," *Int. J. Electr. Power Energy Syst.*, vol. 133, no. 1, Dec. 2021, Art. no. 107277.

[22] F. S. Al-Ismail, "DC microgrid planning, operation, and control: A comprehensive review," *IEEE Access*, vol. 9, pp. 36154–36172, 2021.

[23] H. J. Avelar, W. A. Parreira, J. B. Vieira, L. C. G. de Freitas, and E. A. A. Coelho, "A state equation model of a single-phase grid-connected inverter using a droop control scheme with extra phase shift control action," *IEEE Trans. Ind. Electron.*, vol. 59, no. 3, pp. 1527–1537, Mar. 2012.

[24] N. Pogaku, M. Prodanovic, and T. C. Green, "Modeling, analysis and testing of autonomous operation of an inverter-based microgrid," *IEEE Trans. Power Electron.*, vol. 22, no. 2, pp. 613–625, Mar. 2007.

[25] Z. Wang, S. Li, and Q. Li, "Discrete-time fast terminal sliding mode control design for DC–DC buck converters with mismatched disturbances," *IEEE Trans. Ind. Informat.*, vol. 16, no. 2, pp. 1204–1213, Feb. 2020.

[26] V. Kumar, S. R. Mohanty, and S. Kumar, "Event trigger super twisting sliding mode control for DC micro grid with matched/unmatched disturbance observer," *IEEE Trans. Smart Grid*, vol. 11, no. 5, pp. 3837–3849, Sep. 2020.

[27] H. Khalil and J. W. Grizzle, *Nonlinear Systems*, vol. 3. Upper Saddle River, NJ, USA: Prentice-Hall, 2002.